Spectroscopic and Theoretical Studies on Solid 1,2-Ethylenediamine Dihydrochloride Salt

Ana M. Amado,*[a] Juan Carlos Otero,[b] M. Paula M. Marques,[a] and Luís A. E. Batista de Carvalho[a]

A structural study of $[H_3N(CH_2)_2NH_3]^{2+} \cdot 2Cl^-$, the smallest element of the homologous series of the α,ω-diamine dihydrochlorides, was carried out by means of Raman and FTIR spectroscopy coupled to ab initio molecular orbital (MO) calculations. As a primary concern, an adequate molecular model for the representation of these solid amine salts was chosen. Thus, several models, varying in the number and position of the counterions as well as in the number of diamine units, were considered. It was found that the best molecular system (i.e., that yielding the best compromise between accuracy and computational requirements) consists of one ethylenediamine cation surrounded by six chloride ions in an arrangement based on the crystal structure reported in the literature for $[H_3N(CH_2)_2NH_3]^{2+} \cdot 2Cl^-$. This conclusion will hopefully allow for a better understanding of the conformational preferences, in the solid state, of these biologically relevant linear polyamines.

1. Introduction

Polyamines are found in millimolar concentrations in most living cells, for example, putrescine $[H_2N(CH_2)_4NH_2]$, spermidine $[H_2N(CH_2)_3NH(CH_2)_4NH_2]$ and spermine $[H_2N(CH_2)_3NH(CH_2)_4NH(CH_2)_3NH_2]$. They are N-protonated at physiological conditions, thus behaving as intrinsic polycations. These important biogenic compounds are known to be implicated in a bewildering maze of cellular functions,[1–6] many of them being essential for eukaryotic cell growth and differentiation, as well as for maintaining the native structure of several biological macromolecules, while affecting the activity of others.[6,7] Their interaction with the DNA molecule, for instance, has been widely investigated through different experimental techniques.[8–14]

While deregulated amine metabolism is a well-recognized characteristic of animal and human cancers,[15,16] interference with polyamine biosynthesis is presently a rather promising therapeutical approach against proliferative diseases. Moreover, many efforts have lately been devoted to the possible use of polyamines as biochemical markers of cancer.[6,15,17,18] In addition, it was verified that linkage of some of these molecules to previously tested anticancer drugs leads to a higher cytotoxic effect and, in some cases, even to an enhancement of the efficacy of the long-used first-generation drug cisplatin [cis-diamine dichloroplatinum(II)].[19–27] Recently, it was also demonstrated that polyamines may exert insulinlike activity by interacting with receptors on fat-cell membranes.[28]

Despite the vital role of polyamines in living cells, little is known about their structure at a molecular level. Actually, the understanding of the factors that govern the conformational preferences of these polycationic systems (namely, intra- and/or intermolecular interactions) is of utmost importance for determining the structure–activity relationships (SARs) underlying their biological function. Nevertheless, although ab initio molecular orbital calculations have proved to be a particularly valuable tool for the conformational analysis of amines,[29–37] no such systematic study has, to date, been reported on biogenic polyamine salts. In fact, to the best of the authors' knowledge, only two studies can be found in the literature on the ab initio assignment of the Raman spectra of such molecules, and even these are restricted to the N–H and C–H stretching modes.[38,39]

The present work is aimed at the study of the homologous series of α,ω-diamine dihydrochlorides of general formula $[H_3N(CH_2)_nNH_3]^{2+} \cdot 2Cl^-$ ($n=2$–10 and $n=12$) in the solid state. In the absence of any theoretical report on these polycationic molecules, the primary concern was the selection of an adequate molecular model for the representation of such systems. Therefore, this report comprises the results obtained for the smallest element of the series—1,2-ethylenediamine dihydrochloride, $[H_3N(CH_2)_2NH_3]^{2+} \cdot 2Cl^-$, hereafter named 1,2NH$_3$·Cl— which may subsequently be used as an accuracy measure for the study of even-membered alkyl diamine salts.

2. Results and Discussion

2.1. Structural Analysis

The crystal structure of ethylenediamine dichloride was first obtained by Ashida and Hirokawa,[40] and has recently been refined by Bujak et al.[41] The unit cell contains half an $[NH_3(CH_2)_2NH_3]^{2+}$ cation and one Cl^- anion. Each Cl^- ion is involved in three N–H···Cl hydrogen bonds with three neighboring amine cations (Figure 1). This hydrogen-bond network gives rise to a stacked layered structure, which is kept together

[a] Dr. A. M. Amado, Prof. M. P. M. Marques, L. A. E. Batista de Carvalho
    Química-Física Molecular, Departamento de Química
    FCTUC, Universidade de Coimbra, 3004–535 Coimbra (Portugal)
    Fax: (+351) 239-826541
    E-mail: ama1@portugalmail.pt

[b] Prof. J. C. Otero
    Departamento de Química Física, Facultad de Ciencias
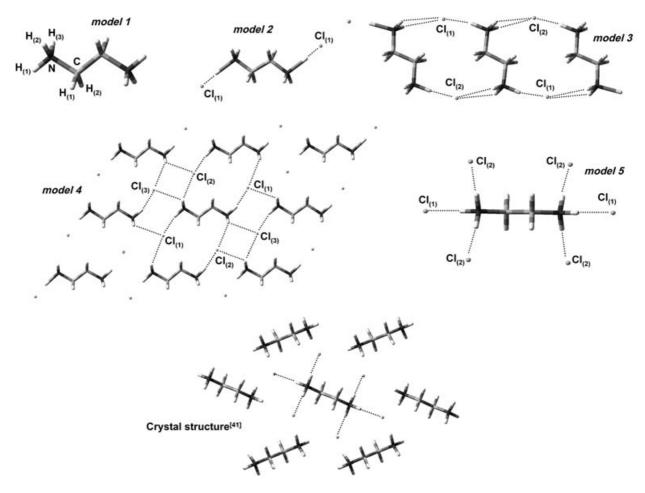   Universidad de Málaga, 29071 Málaga (España)

Figure 1. Schematic representation of the molecular models tested in the present study (both the atom labeling and the model nomenclature are included). A schematic representation of the X-ray structure reported in ref. [41] is shown for an easy comparison.

through additional interlayer [NH₃(CH₂)₂NH₃]²⁺···Cl⁻ close contacts.

Table 1 lists the structural parameters calculated for $1,2NH_3 \cdot Cl$ in the light of the distinct proposed molecular models—*models 1 to 5* (see Experimental Section). Reported experimental values are also included for comparison purposes. The smallest model considered (*model 1*; Figure 1) represents the isolated 1,2-ethylenediamine cation, without any counterion. The absence of the counterions clearly leads to an exaggerated accumulation of positive charge, particularly at the NH_3^+ terminals. As a consequence, several calculated bond lengths are greatly overestimated: the skeletal N–C and C–C bonds by more than 3 pm, and

Table 1. Selected calculated structural parameters (B3LYP/6–31G* level) for $1,2NH_3 \cdots Cl$ in the light of the five molecular models considered. Experimental values from the literature[41] are included for accuracy evaluation purposes.

Structural Parameter	Calcd.[a]					Exptl.
	model 1	model 2	model 3	model 4	model 5	
bond distances [pm]						
N–C	151.8	147.2	149.1	149.1	150.4	148.5
N–H$_{(1)}$	103.4	165.0	109.4	106.3	104.9	84.5
N–H$_{(2,3)}$	103.2	102.0	102.6	102.6	105.7	94.5[b]
C–C	154.2	153.5	152.7	152.5	153.5	151.0
C–H$_{(1,2)}$	109.4	109.7	109.2	109.1	109.3	101.8[b]
bond angles [°]						
N–C–C	110.8	114.6	111.8	111.9	111.9	109.9
H$_{(1)}$–N–C	110.1	108.5	107.0	107.4	109.1	111.4
H$_{(2,3)}$–N–C	113.2	111.3	112.5	114.3	112.5	111.9[b]
H$_{(1)}$–N–H$_{(2,3)}$	106.3	109.2	110.8	109.0	107.3	106.4[b]
H$_{(2)}$–N–H$_{(3)}$	107.4	107.2	103.2	102.5	108.1	108.6
N–C–H$_{(1,2)}$	106.3	107.4	107.1	107.1	107.5	108.5[b]
C–C–H$_{(1,2)}$	112.1	110.2	112.0	112.2	110.5	109.9[b]
H$_{(1)}$–C–H$_{(2)}$	108.9	106.7	106.5	106.0	108.9	108.1
hydrogen-bond distances [pm]						
NH$_{(1)}$···Cl$_{(1)}$	–	137.2	187.6	200.6	242.9	234.0
NH$_{(2,3)}$···Cl$_{(2)}$	–	–	262.2	272.5	224.9	223.8[b]

[a] Nomenclature and atom labeling in accordance with Figure 1. [b] Average value.

the C–H bonds by about 7 pm. The largest discrepancy, however, is observed for the N–H bonds: N–H$_{(1)}$ is calculated almost 19 pm too long, while the out-of-plane N–H bonds [N–H$_{(2)}$ and N–H$_{(3)}$] are overestimated by about 9 pm.

Aiming at overcoming these inadequacies in the theoretical calculations, different molecular models varying in the number of 1,2 NH$_3{}^{2+}$ units, as well as in the number and position of the counterions, were investigated. The simplest of these models—*model 2* (Figure 1)—considers only one 1,2 NH$_3{}^{2+}$ cation, hydrogen bonded to two chloride ions that are collinear with the in-plane N–H$_{(1)}$ bonds. According to the structural data presented in Table 1, the inclusion of the chloride ions at these positions does not improve the prediction of the N–H$_{(1)}$ bond distance, which displays a considerable lengthening (by more than 80 pm). The NH$_{(1)}$···Cl$_{(1)}$ intermolecular distance, in contrast, is underestimated by more than 96 pm. The magnitude of these bond distances indicates that, in this model, the H$_{(1)}$ atom may no longer be seen as covalently bound to the nitrogen, but has moved closer to the chloride anion instead. While both the skeletal and the out-of-plane N–H distances are slightly better approximated in *model 2*, the description of the associated bond angles is clearly defective. The skeletal N–C–C bond angle, for instance, which was closely predicted by *model 1*, becomes overestimated by almost 5° in *model 2*. A similar effect is observed for the two H$_{(1)}$–N–H bond angles, while the opposite occurs for the H–C–H angles.

The theoretical deficiencies displayed by *model 2* are probably related to the excessively localized effect of the chloride counterions. Actually, the analysis of the atomic charges predicted by natural bond order (NBO) calculations supports this conclusion, as it yields a charge of −0.41 at the Cl⁻ ion instead of the expected −1 charge of this counterion. In other words, the chloride ion seems to loose about 0.6 of its electronic charge by interacting with the amine cation. This charge transfer occurs mainly to the H$_{(1)}$ atom (Figure 1), for which the NBO calculations predict a net charge variation of approximately −0.22 relative to the corresponding charge in *model 1*. These deficiencies render both molecular *models 1* and *2* inadequate for a rigorous prediction of the structural features of alkyl diamine salts in the solid state.

In the light of the two main characteristics of the crystal structure of 1,2 NH$_3$·Cl—the involvement of all NH$_3{}^+$ groups in NH···Cl close contacts and the presence of three such contacts per chloride ion—two larger molecular models were built, which correspond to the trimeric (*model 3*) and nonameric (*model 4*) forms of *model 2* (Figure 1). In these models, the description of the N–H$_{(1)}$ bond distance is considerably improved compared to *models 1* and *2*, although it is still overestimated by 24.9 and 21.8 pm in *models 3* and *4*, respectively. The NH$_{(1)}$···Cl bond distance, in turn, becomes closer to its experimental value, its overestimation being reduced to 46.4 and 33.4 pm in *models 3* and *4*, respectively. Moreover, the calculated NBO atomic charges at the H$_{(1)}$ and Cl atoms become more accurate: they increase to 0.44 and 0.46 for H$_{(1)}$ and decrease to −0.80 and −0.84 for Cl, in *models 3* and *4*, respectively.

While some other structural parameters are also improved by *models 3* and *4* (e.g., the skeletal bond distances and angles, and the C–H bond distances), not all are accurately represented. The most evident discrepancy occurs for the description of the two NH$_{(2,3)}$···Cl close contacts. The H$_{(2,3)}$···Cl distances are greatly overestimated by both molecular models: while they are calculated to be significantly longer than the NH$_{(1)}$···Cl distance, the experimental values indicate the opposite.

Aiming at a further improvement of the representation of the 1,2 NH$_3$·Cl solid system, another molecular model was proposed based on the reported crystal structure for 1,2 NH$_3$·Cl[40,41]—*model 5* (Figure 1). This model considers a diamine cation surrounded by six chloride ions, each one pointing to an NH group (Figure 1), as it is known to occur in the crystal. Calculations based on this model lead to greatly improved geometrical parameters, the only exceptions being the skeletal and out-of-plane N–H bond distances, which become overestimated by 1.9 (N–C), 2.4 (C–C), and 11.3 pm (N–H$_{(2,3)}$). In addition, despite a slight improvement, N–H$_{(1)}$ remains overestimated by 20.4 pm. *Model 5* yields a particularly significant refinement in the description of the NH···Cl close contacts. Not only is their overestimation greatly reduced, but also their relative order of magnitude becomes coincident with the experimental one (NH$_{(2,3)}$···Cl < NH$_{(1)}$···Cl).

On the whole, the above-described results clearly show that both the number and localization of the Cl⁻ counterions relative to the diammonium cation are of the utmost importance for an accurate representation of the 1,2 NH$_3$·Cl system. Keeping in mind that the theoretical calculations refer to the isolated system while the experimental results concern a condensed phase, *model 5* proved to be suitable for the simulation of the 1,2 NH$_3$·Cl salt in the solid state. The remaining deficiencies might result from a misrepresentation of the interlayer NH···Cl and CH···Cl interactions, which are known to occur in the solid.[40,41]

2.2. Vibrational Analysis

The 1,2 NH$_3$·Cl molecule displays 42 normal modes of vibration, from which 36 are related to the diamine cation, and the remaining six are related to the interaction with the chloride counterions. In the all-*trans* configuration (C_{2h} symmetry) the 36 diamine modes are distributed as follows: $11A_g + 7B_g + 8A_u + 10B_g$. Thus, 18 Raman-active and 18 IR-active mutually exclusive fundamental modes are expected.

Although several experimental studies are to be found in the literature concerning the vibrational assignment of solid 1,2-ethylenediamine dihydrochloride,[42–46] there is strong disagreement between these works.

The assignment of both the Raman and FTIR spectra of 1,2 NH$_3$·Cl is carried out on the basis of the present results on both nondeuterated and N-deuterated samples, as well as on previously reported works for similar systems.[29–31,47–49] The controversies encountered in the reported vibrational assignments for 1,2 NH$_3$·Cl[42–46] are considered. Furthermore, the theoretical accuracy of the five proposed molecular models in reproducing the vibrational spectra of 1,2 NH$_3$·Cl is discussed. This study will hopefully help to shed some light on several

questions still unanswered for this type of solid systems, namely, the relative wavenumber order of particular vibrational modes (as discussed further).

2.2.1 Theoretical Vibrational Frequencies

Model 5, which has been shown to be the best model for simulating the 1,2 NH$_3$·Cl structure, is also expected to yield the most accurate vibrational frequencies. Table 2 contains the calculated wavenumbers and approximate assignments predicted for both the 1,2 NH$_3$·Cl and 1,2 ND$_3$·Cl isotopomers in the light of *model 5*. The corresponding potential energy distribution (PED) values and isotopic shifts ($\Delta\tilde{\nu}$) are also included.

The PED calculations evidence a significant mixture of internal coordinates describing the vibrational modes, particularly the low-wavenumber fundamentals for both isotopomers. This complex mixing renders the assignment of one wavenumber to one internal coordinate difficult in some cases; moreover, it leads to an almost overall frequency shift when going from 1,2 NH$_3$·Cl to 1,2 ND$_3$·Cl (with most frequency vibrational bands displaying significant isotopic shifts, $\Delta\tilde{\nu}$ values).

Table 3 contains the B3LYP/6–31G* calculated vibrational wavenumbers for 1,2 NH$_3$·Cl, obtained on the basis of the five molecular models tested, along with the corresponding experimental values. Visualizing the atomic displacements makes the wavenumber correspondence between different molecular models evident, and the analysis of the results allows the determination of the most significant deficiencies of each molecular model tested.

The tentative assignments presented in Table 3 are based on the largest PED value shown in Table 2. This correlation principle, however, fails in some cases, as no internal coordinate is found to be dominant. This is the case for the calculated mode at 902 cm^{-1} (A_g symmetry), which is predicted to have similar contributions from three different oscillators: 28% $\tilde{\nu}_{NC}$, 22% $\tilde{\nu}_{CC}$, and 22% δ_{NCC}. The 902 cm^{-1} wavenumber was tentatively ascribed to the missing $\tilde{\nu}_{CC}$ mode, while the 449 and 1007 cm^{-1} wavenumbers (A_g symmetry) were predicted to

Table 2. *Calculated wavenumbers for 1,2 NH$_3$·Cl and 1,2 ND$_3$·Cl isotopomers, based on model 5. The calculated PED values,[a] wavenumber shifts upon N-deuteration, and assignments are included.*

sym	1,2 NH$_3$·Cl		1,2 ND$_3$·Cl		
	$\tilde{\nu}$[b] [cm^{-1}]	PED[c] [%]	$\tilde{\nu}$[b] [cm^{-1}]	PED[c] [%]	$\Delta\tilde{\nu}$[d] [cm^{-1}]
A_g	449	$58\delta_{NCC}+14\tilde{\nu}_{NC}$	414	$56\delta_{NCC}+14\tilde{\nu}_{NC}+14\tau_{CN}$	35
	902	$28\tilde{\nu}_{NC}+22\tilde{\nu}_{CC}+22\delta_{NCC}$	765	$36\rho_{ND_3}+20\tau_{CN}+16\tilde{\nu}_{CC}$	137
	1007	$56\tilde{\nu}_{NC}+37\tilde{\nu}_{CC}$	965	$58\tilde{\nu}_{NC}+13\tilde{\nu}_{CC}+14\delta_{NCC}$	42
	1223	$46\rho_{NH_3}+18\tau_{CN}$	1085	$43\tilde{\nu}_{CC}+20\delta_{NCC}+20\rho_{ND_3}$	138
	1401	$76\omega_{CH_2}+11\tilde{\nu}_{CC}$	1395	$88\omega_{CH_2}+10\tilde{\nu}_{CC}$	6
	1468	$94\delta_{CH_2}$	1468	$96\delta_{CH_2}$	0
	1566	$78\delta_{sNH_3}+18\tau_{CN}$	1188	$70\delta_{sND_3}+14\tau_{CN}+12\tilde{\nu}_{NC}$	378
	1637	$72\delta_{asNH_3}+16\tau_{NH}$	1174	$70\delta_{asND_3}+16\tau_{ND}$	463
	2854	$96\tilde{\nu}_{NH_3}$	2060	$98\tilde{\nu}_{ND_3}$	794
	2977	$86\tilde{\nu}_{NH_3}+12\tilde{\nu}_{CH_2}$	2193	$96\tilde{\nu}_{ND_3}$	784
	2980	$84\tilde{\nu}_{CH_2}+16\tilde{\nu}_{NH_3}$	2979	$100\tilde{\nu}_{CH_2}$	1
B_g	552	$88\tau_{NH}$	391	$88\tau_{ND}$	161
	950	$46\rho_{CH_2}+22\rho_{NH_3}$	772	$46\rho_{ND_3}+20\delta_{NH_3}+12\tau_{ND}$	178
	1248	$36\rho_{CH_2}+34\rho_{NH_3}$	1143	$72\rho_{CH_2}$	105
	1315	$82t_{CH_2}$	1301	$94t_{CH_2}$	14
	1643	$74\delta_{asNH_3}+16\tau_{NH}$	1178	$72\delta_{sND_3}+16\tau_{ND}$	465
	2851	$96\tilde{\nu}_{NH_3}$	2114	$96\tilde{\nu}_{ND_3}$	737
	3026	$100\tilde{\nu}_{CH_2}$	3026	$100\tilde{\nu}_{CH_2}$	0
A_u	234	$48\tau_{CC}+16\tau_{CN}+16\tau_{NH}$	210	$46\tau_{CC}+20\tau_{CN}$	24
	547	$88\tau_{NH}$	387	$86\tau_{ND}$	160
	771	$68\rho_{CH_2}+12\tau_{CC}$	736	$52\rho_{CH_2}+15\tau_{CC}+16\rho_{ND_3}$	35
	1051	$38t_{CH_2}+34\rho_{NH_3}$	862	$36\rho_{ND_3}+26t_{CH_2}+18\rho_{CH_2}$	189
	1321	$44t_{CH_2}+24\rho_{NH_3}$	1253	$74t_{CH_2}$	68
	1645	$72\delta_{asNH_3}+16\tau_{NH}$	1175	$74\delta_{asND_3}+18\tau_{ND}$	470
	2855	$96\tilde{\nu}_{NH_3}$	2118	$96\tilde{\nu}_{ND_3}$	737
	3045	$100\tilde{\nu}_{CH_2}$	3045	$100\tilde{\nu}_{CH_2}$	0
B_u	330	$62\delta_{NCC}+28\tau_{CN}$	300	$60\delta_{NCC}+30\tau_{CN}$	30
	952	$98\tilde{\nu}_{NC}$	910	$90\tilde{\nu}_{NC}$	42
	1109	$46\rho_{NH_3}+26\tau_{CN}$	859	$60\rho_{ND_3}+28\tau_{CN}$	250
	1342	$74\omega_{CH_2}+14\rho_{NH_3}$	1313	$92\omega_{CH_2}$	29
	1479	$94\delta_{CH_2}$	1479	$94\delta_{CH_2}$	0
	1567	$78\delta_{sNH_3}+18\tau_{CN}$	1188	$72\delta_{sND_3}+18\tau_{CN}+12\tilde{\nu}_{NC}$	379
	1633	$72\delta_{asNH_3}+20\tau_{NH}$	1169	$78\delta_{asND_3}+20\tau_{ND}$	464
	2842	$96\tilde{\nu}_{NH_3}$	2049	$96\tilde{\nu}_{ND_3}$	793
	2974	$98\tilde{\nu}_{NH_3}$	2191	$100\tilde{\nu}_{ND_3}$	783
	2988	$100\tilde{\nu}_{CH_2}$	2988	$100\tilde{\nu}_{CH_2}$	0

[a] Table of symmetry internal coordinates and corresponding figure are available from the authors upon request. [b] Calculated vibrational frequencies (B3LYP/6–31G*) using *model 5* for the 1,2 NH$_3$·Cl and 1,2 ND$_3$·Cl isotopomers; frequencies above 500 cm^{-1} are scaled by 0.9614.[63] [c] $\tilde{\nu}$ = stretching; δ = bending; ρ = rocking; ω = wagging; t = twisting; τ = torsion; s = symmetric; as = antisymmetric. [d] $\Delta\tilde{\nu} = \tilde{\nu}_{1,2 NH_3·Cl} - \tilde{\nu}_{1,2 ND_3·Cl}$

Table 3. *Comparison of the calculated vibrational frequencies (B3LYP/6–31G* level) for 1,2NH₃···Cl, determined in the light of the five molecular models tested, with the experimentally observed values. The vibrational isotopic shifts (Δṽ values) predicted with model 5 are also compared with the experimental values observed. The assignments are based on the calculated atomic displacements and on the PED values presented in Table 2.*

| Sym | Calculated $\tilde{\nu}^{[a]}$ [cm⁻¹] | | | | | Δṽ | Experimental $\tilde{\nu}$ [cm⁻¹] | | | Assignment[b] |
	model 1	model 2	model 3	model 4	model 5		Raman	FTIR	Δṽ	
A_g	423	478	472	466	449	35	464		34	δ_{NCC} (LAM1)
	835	772	898	1026	902	137	922		126	$\tilde{\nu}_{CC}$
	973	1073	1027	1025	1007	42	1053		49	$\tilde{\nu}_{NC}$
	1156	1039	1188	1171	1223	138	1210		180	ρ_{NH_3}
	1426	1376	1407	1411	1401	6	1419		8	ω_{CH_2}
	1461	1455	1450	1443	1468	0	1491		1	δ_{CH_2}
	1530	972	1497	1490	1566	378	1609			δ_{sNH_3}
	1628	1624	1594	1602	1637	463	1632		454	δ_{asNH_3}
	3221	3341	3302	3319	2854	794	2807		[c]	$\tilde{\nu}_{sNH_3}$
	3284	1828	2316	2728	2977	784	2899		[c]	$\tilde{\nu}_{asNH_3}$
	2978	2938	3001	3005	2980	1	2913		5	$\tilde{\nu}_{sCH_2}$
B_g	249	387	321	277	552	161	469		134	τ_{NH}[d]
	879	846	878	835	950	178	940		171	ρ_{NH_3}
	1204	962	1221	1192	1248	105	1246		133	ρ_{CH_2}
	1334	1256	1308	1307	1315	14	1333		8	t_{CH_2}
	1633	1336	1567	1587	1643	465	1611		465	δ_{asNH_3}
	3297	3423	3343	3353	2851	737	2818		[c]	$\tilde{\nu}_{asNH_3}$
	3031	2973	3041	3045	3026	0	2977		0	$\tilde{\nu}_{asCH_2}$
A_u	116	131	72	73	234	24			–	τ_{CC}
	221	369	308	260	547	160			–	τ_{NH}[d]
	759	735	747	724	771	35		819	58	ρ_{CH_2}
	983	883	989	949	1051	189		1031	176	ρ_{NH_3}
	1326	1053	1315	1299	1321	68		1343	56	t_{CH_2}
	1635	1357	1570	1597	1645	470		1610	440	δ_{asNH_3}
	3297	3423	3344	3354	2855	737		2874	[c]	$\tilde{\nu}_{asNH_3}$
	3048	2996	3061	3066	3045	0		2972	[c]	$\tilde{\nu}_{asCH_2}$
B_u	273	324	389	335	330	30			–	δ_{NCC} (LAM2)
	911	1027	976	977	952	42		1007	36	$\tilde{\nu}_{NC}$
	1016	813	1073	1041	1109	250		1085	189	ρ_{NH_3}
	1365	1310	1348	1349	1342	29		1361	25	ω_{CH_2}
	1469	1470	1459	1453	1479	0		1486	1	δ_{CH_2}
1531	993	1492	1489	1567	379		1501	414		δ_{sNH_3}
	1623	1623	1589	1590	1633	464		1601	448	δ_{asNH_3}
	3216	3340	3301	3318	2842	793		2799	[c]	$\tilde{\nu}_{sNH_3}$
	3284	1779	2273	2711	2974	783		2899	[c]	$\tilde{\nu}_{asNH_3}$
	2986	2947	3009	3015	2988	0			–	$\tilde{\nu}_{sCH_2}$
r.m.s[e]	1080	2190	1344	1113	237					

[a] Molecular models nomenclature in accordance with Figure 1; calculated frequencies above 500 cm⁻¹ are scaled by 0.9614.[63] [b] $\tilde{\nu}$ = stretching; δ = bending; ρ = rocking; ω = wagging; t = twisting; τ = torsion; s = symmetric; as = antisymmetric; LAM = longitudinal acoustic mode. [c] Not determined due to the strong overlapping of bands (see text). [d] See text for description of the mode. [e] Root-mean square: $\sqrt{\sum [(\tilde{\nu}_i(\text{exptl.}) - \tilde{\nu}(\text{theor.}))^2]}$

have high contributions from the δ_{NCC} (58%) and $\tilde{\nu}_{NC}$ (56%) co-ordinates, respectively.

The 1051 cm⁻¹ wavenumber (A_u symmetry), in turn, comprises contributions from t_{CH_2} (38%) and ρ_{NH_3} (34%). As the t_{CH_2} contribution to the 1321 cm⁻¹ band is higher (44%) (which allows the assignment of this wavenumber to the t_{CH_2} mode), the 1051 cm⁻¹ wavenumber is ascribed to the ρ_{NH_3} mode. This assignment is corroborated by the Δṽ value predicted for both wavenumbers, which is larger for the fundamental at 1051 cm⁻¹, as expected for a ρ_{NH_3} mode ($\Delta\tilde{\nu}_{1051}$ = 189 cm⁻¹ vs. $\Delta\tilde{\nu}_{1321}$ = 68 cm⁻¹).

A different situation occurs for the mode at 950 cm⁻¹ (B_g symmetry). The PED calculations predict a large contribution from the ρ_{CH_2} coordinate (46%) and a rather smaller one from ρ_{NH_3} (22%). In contrast, the 1248 cm⁻¹ wavenumber (B_g symmetry) shows similar terms from both coordinates (36 and 34%,

respectively). Thus, on the basis of the larger PED contribution, the 950 cm⁻¹ wavenumber would be assigned to the ρ_{CH_2} mode, and the band at 1248 cm⁻¹ to the ρ_{NH_3} mode. However, if the Δṽ values are taken into account, an opposite assignment (ρ_{NH_3} at 950 cm⁻¹ and ρ_{CH_2} at 1248 cm⁻¹) becomes more reasonable.

An interesting feature, evidenced by both the PED calculations and the vibrational atomic displacements, is the prediction of two types of NH₃ torsional modes. The calculated frequencies at 547 and 552 cm⁻¹ (A_u and B_g symmetry, respectively) correspond to the τ_{NH} modes in which the N–H groups seem to exchange the counterion (Cl⁻) involved in the N–H···Cl close contact. Strictly speaking, this torsion (τ_{NH}) occurs around the central N–H bond in the C–N–H–Cl moiety.

In the other type of NH₃ torsion (hereafter named τ_{CN}), the chloride counterions seem to accompany the movement of

the corresponding N—H group in its rotation around the N—C bond. These τ_{CN} modes are predicted to appear at much lower frequencies in both Raman and IR, namely, at 104 (B_g symmetry) and 14 cm^{-1} (A_u symmetry), respectively.

Comparison between experimental and theoretical results confirms that *model 5* is by far the molecular model that yields the best vibrational wavenumber accuracy, as it presents the lowest overall root-mean-square (r.m.s.) value (Table 3). *Model 1*, for instance, presents an r.m.s. of 1080 cm^{-1} and is particularly ineffective in reproducing the frequency of the NH$_3$ stretching modes, which are greatly overestimated (by more than 400 cm^{-1}). On the contrary, the Raman wavenumber of the NH$_3$ torsion mode is underestimated by more than 200 cm^{-1}.

Model 2 clearly worsens the overall agreement between experimental and theoretical frequencies, the r.m.s. value drastically increasing to 2190 cm^{-1}. Although a slight improvement occurs in the prediction of the Raman-active τ_{NH} mode (underestimation is reduced to 82 cm^{-1}), the calculation of the $\tilde{\nu}_{NH_3}$ mode is much less accurate. In fact, the overestimation of both the symmetric and antisymmetric NH$_3$ stretching modes (one Raman active and one IR active) is further increased. Moreover, the excessively localized effect of the chloride counterions over the N—H$_{(1)}$ groups, as previously stated, leads to an exaggerated underestimation (by more than 1000 cm^{-1}) of the two remaining antisymmetric $\tilde{\nu}_{NH_3}$ vibrations. Finally, this model is also particularly inefficient in predicting the δ_{NH_3} modes, which are greatly underestimated.

Increasing complexity up to *models 3* and *4* (Figure 1) does not overcome these drawbacks. Despite a significant decrease of the overall r.m.s. relative to *model 2*, its value remains higher than that presented by *model 1*. This high r.m.s. value is mainly due to the overestimation of $\tilde{\nu}_{NH_3}$ and, particularly, to the underestimation of τ_{NH}.

Regarding the structural accuracy evaluation, *model 5* presents the lowest overall r.m.s. value. The largest theoretical/experimental discrepancy occurs in the prediction of the Raman-active τ_{NH} mode, which is overestimated by almost 100 cm^{-1} (the accuracy in the prediction of the IR-active τ_{NH} could not be assessed, as this mode was not observed experimentally). This deficiency may result from the fact

that the interlayer NH···Cl and CH···Cl close contacts, which are known to occur in the solid structure of 1,2NH$_3$·Cl, are not taken into account by this model. Nevertheless, the results obtained in the light of *model 5* are undoubtedly the best compromise between accuracy and computational requirements. Moreover, this result evidences the relevance of both the number and spatial disposition of the Cl$^-$ counterions around the [1,2NH$_3$]$^{2+}$ fragment to the accuracy of the calculations.
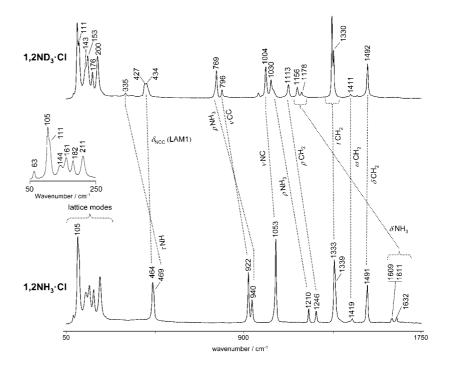

Figure 2. Raman spectra (50–1750 cm^{-1}) for 1,2-ethylenediamine dihydrochloride in its undeuterated (1,2NH$_3$·Cl) and N-deuterated (1,2ND$_3$·Cl) forms. The inset shows the dispersive Raman spectra in the low-wavenumber region (50–250 cm^{-1}) for 1,2NH$_3$·Cl (see text).
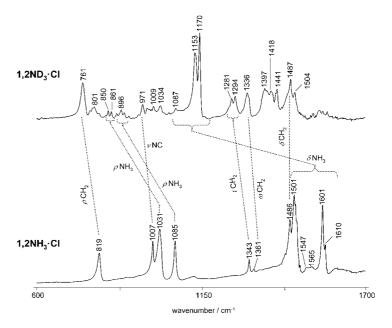

Figure 3. FTIR-ATR spectra (600–1700 cm^{-1}) for 1,2-ethylenediamine dihydrochloride in its undeuterated (1,2NH$_3$·Cl) and N-deuterated (1,2ND$_3$·Cl) forms.

2.2.2. Experimental Vibrational Spectra

Figures 2 and 3 show the FT-Raman (50–1750 cm^{-1}) and the FTIR-ATR (attenuated total reflection) (600–1750 cm^{-1}) spectra of solid 1,2 NH$_3$·Cl and 1,2 ND$_3$·Cl, respectively. The inset of Figure 2 displays the low-wavenumber region (50–250 cm^{-1}) of the dispersive Raman spectrum. Apart from some relative intensity changes, no meaningful differences (besides the quality of the baseline) were observed above 100 cm^{-1} between the
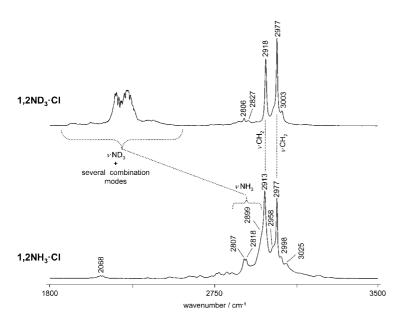
FT-Raman and the dispersive Raman spectra. Figures 4 and 5 show the FT-Raman and FTIR-ATR spectra of the two isotopomers in the 1800–3500 cm^{-1} region. The noncoincidence between the Raman and IR spectral features is obvious.

In this section, a full spectral assignment is performed for both isotopomers in the light of the theoretical results obtained with molecular *model 5*. The controversies encountered in the literature[42–46] are discussed on the basis of those theoretical results.

Spectral region below 250 cm^{-1}: This spectral region is characterized by the presence of several bands ascribed to lattice modes. The dispersive Raman spectrum shows an additional low-wavenumber band at 63 cm^{-1} (see inset of Figure 2).

Deuteration of the amino groups leads to small shifts of all Raman bands except for two: the shoulders at about 111 and 143 cm^{-1}. These spectral features give rise to well-defined features at the same wavenumber in the 1,2 ND$_3$·Cl spectrum as a result of a shift of the close-lying intense bands at 105 and 161 cm^{-1} to 103 and 153 cm^{-1}, respectively, in the 1,2 ND$_3$·Cl spectrum. These low-wavenumber modes are related to the interaction of the diamine cation with the chloride counterions in the crystalline network. The theoretical calculations based on *model 5* also indicate that the Raman-active τ_{CN} mode occurs around 104 cm^{-1}.

Spectral region 300–500 cm^{-1}: In the 300 to 500 cm^{-1} wavenumber range, two vibrational Raman-active modes are expected, namely, the skeletal deformation (δ_{NCC}) and the torsion of the NH$_3$ groups (τ_{NH}). In turn, the Raman spectrum shows a single band in this region (at 464 cm^{-1}), which displays a shoulder at about 469 cm^{-1} (Figure 2). The assignment of these two spectral features to one of those oscillators (δ_{NCC} or τ_{NH}) is controversial. In fact, while both McLachlan,[44] and Mureinik and Scheuermann[42] assigned the strongest feature to the δ_{NCC} vibration and the shoulder to the τ_{NH} mode, Angeloni et al.[45] reported an opposite assignment.

Based on the theoretical results presented, the δ_{NCC} mode is predicted to have a lower wavenumber than τ_{NH}. Thus, the band at 464 cm^{-1} is ascribed to the skeletal deformation mode (δ_{NCC}), while the τ_{NH} mode is correlated to the shoulder observed at 469 cm^{-1}. This assignment is supported by the N-deuteration study (Figure 2). Actually, the disappearance of the band pair 464/469 cm^{-1} upon N-deuteration, coupled to the detection of a weak feature at about 335 cm^{-1} and a doublet at 427 and 434 cm^{-1} for 1,2 ND$_3$·Cl, evidences the occurrence of both δ_{NCC} and τ_{NH} modes. As τ_{NH} is expected to have a larger red shift upon N-deuteration than the δ_{NCC} mode ($\Delta\tilde{\nu}$ values, Table 2), it seems reasonable to assign the 335 cm^{-1} band to the torsion vibration (this wavenumber being about 1.4 times smaller than that of the shoulder occurring at 469 cm^{-1} in the spectrum of 1,2 NH$_3$·Cl). By exclu-

Figure 4. *Raman spectra (1800–3500 cm^{-1}) for 1,2-ethylenediamine dihydrochloride in its undeuterated (1,2 NH$_3$·Cl) and N-deuterated (1,2 ND$_3$·Cl) forms.*
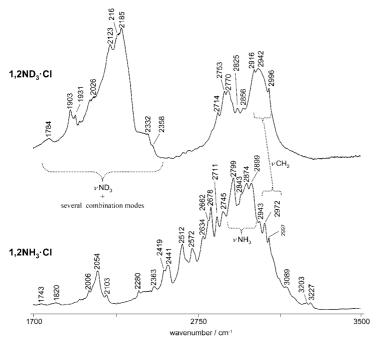

Figure 5. *FTIR-ATR spectra (1800–3500 cm^{-1}) for 1,2-ethylenediamine dihydrochloride in its undeuterated (1,2 NH$_3$·Cl) and N-deuterated (1,2 ND$_3$·Cl) forms.*

sion, the 427/434 cm^{-1} doublet is ascribed to the skeletal deformation in 1,2 ND$_3$·Cl, which corresponds to the downward shift of the δ_{NCC} mode at 464 cm^{-1} in 1,2 NH$_3$·Cl. This assignment also agrees with the criterion of relative intensities, the δ_{NCC} mode giving rise to a stronger feature than the τ_{NH} one. N-deuteration splitting of the δ_{NCC} band has been previously reported for liquid *n*-propylamine,[47] and has been correlated to the occurrence of different conformers (*trans/gauche* equilibrium due to rotation around the NC–CC bond). For solid 1,2 ND$_3$·Cl salt, however, the all-*trans* geometry is expected to prevail. Thus, in the present case, it seems more plausible that N-deuteration enhances the crystal packing splitting effect, which leads to the observation of two individualized bands at 427 and 434 cm^{-1} (the second band probably being overlapped with the low-intensity τ_{NH} mode in the spectrum of 1,2 NH$_3$·Cl).

Spectral region 750–1800 cm^{-1}: The Raman band pair observed at 922 and 940 cm^{-1} (Figure 2) was previously assigned by Mureinik and Scheuermann[42] to a rocking vibration of the NH$_3$ group (ρ_{NH_3}) and to the stretching mode of the skeletal C–C bond ($\tilde{\nu}_{CC}$), respectively. More recently, both McLachlan[44] and Angeloni et al.[45] ascribed these bands to the Raman-active ρ_{NH_3} modes expected for 1,2 NH$_3$·Cl.

The theoretical results now presented (Tables 2 and 3) point to an assignment close to that of Mureinik and Scheuermann,[42] although suggesting the opposite wavenumber-to-mode correlation: the band at 922 cm^{-1} is assigned to the $\tilde{\nu}_{CC}$ mode and that at 940 cm^{-1} is associated to the ρ_{NH_3} oscillator. N-deuteration leads to a red shift of both bands to 796 ($\Delta\tilde{\nu} = 126$ cm^{-1}) and 769 cm^{-1} ($\Delta\tilde{\nu} = 171$ cm^{-1}), respectively (the $\Delta\tilde{\nu}$ values being relatively well predicted theoretically—137 and 178 cm^{-1}, respectively). As referred to previously, this double wavenumber shift is explained on the basis of the mixed PED description of both modes (Table 2).

In the FTIR spectrum of 1,2 NH$_3$·Cl, only one band is detected below 900 cm^{-1} (at 819 cm^{-1}, Figure 3). This band was previously attributed to the ρ_{CH_2} vibration.[43,45,46] The present theoretical results support this assignment and predict a red shift of 35 cm^{-1} upon N-deuteration. On the basis of this result, it is reasonable to correlate the 761 cm^{-1} band in the spectrum of 1,2 ND$_3$·Cl to the 819 cm^{-1} feature in the spectrum of 1,2 NH$_3$·Cl.

In the spectral range between 1000 and 1300 cm^{-1}, three well-defined bands are observed in both the Raman and the FTIR spectra (Figures 2 and 3). The assignment of these features is rather controversial. The 1053 and 1210 cm^{-1} Raman bands, for instance, were reported by both McLachlan[44] and Angeloni et al.[45] to be due to the skeletal stretching modes $\tilde{\nu}_{CC}$ and $\tilde{\nu}_{NC}$, although these authors did not coincide in the wavenumber order of this assignment. The present theoretical results, however, support the assignment of the 1053 cm^{-1} band to the $\tilde{\nu}_{NC}$ mode, as suggested by Angeloni et al.,[45] but relate the 1210 cm^{-1} feature to the second Raman-active ρ_{NH_3} vibration (the $\tilde{\nu}_{CC}$ was predicted to be related to the 922 cm^{-1} band). The calculations also predict $\Delta\tilde{\nu}$ values of 42 and 138 cm^{-1} for these two modes, respectively (Table 2). Based on these values, the bands at 1004 and 1030 cm^{-1} in the spec-

trum of 1,2 ND$_3$·Cl are correlated with the features at 1053 and 1210 cm^{-1}, respectively, which are observed for 1,2 NH$_3$·Cl (Figure 2). Still in accordance with Angeloni et al.,[45] the Raman band at 1246 cm^{-1} is related to the ρ_{CH_2} mode. The calculations support this assignment and suggest a shift to 1113 cm^{-1} upon N-deuteration (experimental $\Delta\tilde{\nu} = 133$ cm^{-1} vs. calculated $\Delta\tilde{\nu} = 105$ cm^{-1}).

Regarding the FTIR spectrum, the 1000–1300 cm^{-1} region comprises bands at 1007, 1031, and 1085 cm^{-1} (Figure 3), apart from some low-intensity shoulders whose occurrence has not been referred to in previous publications.[42,43,45,46] Berg and Rasmussen[43] ascribed the 1031 cm^{-1} band to both the $\tilde{\nu}_{NC}$ and one of the IR-active ρ_{NH_3} modes, and the feature at 1007 cm^{-1} to the second IR-active ρ_{NH_3} vibration. Mureinik and Scheuermann[42] in turn, attribute the two IR-active ρ_{NH_3} modes to the bands at 1007 and 1031 cm^{-1}, and the $\tilde{\nu}_{NC}$ fundamental to the band at 1085 cm^{-1}. The present theoretical results, however, seem to agree with a third proposal of both Angeloni et al.[45] and Oxton and Knop,[46] who state that the two ρ_{NH_3} vibrations correspond to the bands at 1031 and 1085 cm^{-1}, while the $\tilde{\nu}_{NC}$ mode gives rise to the 1007 cm^{-1} band. Both ρ_{NH_3} modes are suggested to be red shifted to 850–890 cm^{-1}, as indicated by the calculated $\Delta\tilde{\nu}$ values (Table 2). The $\tilde{\nu}_{NC}$ mode is expected to undergo a much smaller red shift (ca. 42 cm^{-1}; Table 2). Thus, it is suggested that the band at 1007 cm^{-1} in the 1,2 NH$_3$·Cl spectrum is related to the 971 cm^{-1} feature observed for 1,2 ND$_3$·Cl.

The CH$_2$ groups are expected to yield four Raman-active deformation modes in both the Raman and the FTIR spectra—rocking (ρ_{CH_2}), twisting (t_{CH_2}), wagging (ω_{CH_2}), and scissoring (δ_{CH_2}). The two ρ_{CH_2} modes have already been assigned. The t_{CH_2} and ω_{CH_2} vibrations, in turn, are tentatively ascribed to the Raman features at 1333 and 1419 cm^{-1} (Figure 2), and to the FTIR bands at 1343 and 1361 cm^{-1} (Figure 3), respectively.

The calculated isotopic shifts predict a relatively small downward shift for both the Raman active CH$_2$ modes ($\Delta\tilde{\nu}(t_{CH_2}) = 14$ cm^{-1} and $\Delta\tilde{\nu}(\omega_{CH_2}) = 6$ cm^{-1}) and the IR-active ω_{CH_2} fundamental ($\Delta\tilde{\nu} = 29$ cm^{-1}). Thus, these modes correlate with the 1,2 ND$_3$·Cl Raman bands at 1321/1330 and 1411 cm^{-1} (Figure 2), and with the FTIR band at 1336 cm^{-1} (Figure 3). For the IR-active t_{CH_2} mode, the predicted shift is significantly larger, ($\Delta\tilde{\nu} = 68$ cm^{-1}), which suggests a correlation between the band at 1343 cm^{-1} (1,2 NH$_3$·Cl) and the doublet at 1281/1294 cm^{-1} (1,2 ND$_3$·Cl). As for the δ_{NCC} mode, the band splitting of these modes upon N-deuteration, in both the Raman and the FTIR spectra, is probably due to the isotopic enhancement of the crystal packing effect. For instance, the observation of the Raman-active band at 1333 cm^{-1} (1,2 NH$_3$·Cl) already evidences the presence of a shoulder at about 1339 cm^{-1}, the separation of these two features being probably increased by the isotopic substitution.

The bands at 1491 cm^{-1} (Raman) and 1486 cm^{-1} (FTIR) are ascribed to the δ_{CH_2} vibrations (in disagreement with all previously reported assignments,[42,44,45] which relate these bands to a deformation mode of the NH$_3$ groups). In fact, the N-deuteration effect presently reported does not lead to a downward shift of these spectral features, as would be expected if they

corresponded to a δ_{NH_3} mode. This insensitivity of the δ_{NH_3} wavenumber to isotopic substitution is supported by the force field calculations (Table 2).

The three Raman-active deformation modes—one symmetric and two antisymmetric—expected for the NH_3 groups in the $1,2\,NH_3^{2+}$ cation are ascribed to three weak bands observed at 1609, 1611, and 1632 cm^{-1} (Figure 2). These are expected to be significantly down-shifted upon N-deuteration (the calculated $\Delta\tilde{\nu}$ values are all larger than 350 cm^{-1}). Thus, these modes are suggested to give rise to the spectral features at 1156 and 1178 cm^{-1} in the spectrum of $1,2\,ND_3\cdot Cl$. A similar behavior is observed in the FTIR spectrum for the bands at 1501, 1601, and 1610 cm^{-1}, which are also shifted by a factor of about 1.4 upon deuteration, giving rise to bands between 1080 and 1190 cm^{-1}.

Accurate ab initio calculations are also a valuable tool in distinguishing between the symmetric and antisymmetric vibrational modes. Thus, it was verified that the two δ_{sNH_3} modes have a lower wavenumber than the four δ_{asNH_3} vibrations in both the Raman and the FTIR spectra. Accordingly, the Raman and FTIR bands at 1606 and 1501 cm^{-1}, respectively, are assigned to the δ_{sNH_3} modes. On the other hand, the Raman-active δ_{asNH_3} fundamentals yield the bands at 1611 and 1632 cm^{-1}, while the IR-active ones give rise to the bands at 1601 and 1610 cm^{-1}.

Spectral region 1800–3500 cm^{-1}: This spectral range comprises the stretching modes of the CH_2 and NH_3 groups. Apart from the expected five active bands in both the Raman and FTIR spectra—two $\tilde{\nu}_{asNH_3}$ bands, one $\tilde{\nu}_{sNH_3}$ band, one $\tilde{\nu}_{asCH_2}$ band, and one $\tilde{\nu}_{sCH_2}$ band—several other low-intensity features are observed (Figures 4 and 5). These features are characteristic of this kind of molecular system (amine salts) and are due to different combination modes of the δ_{NH_3} fundamentals.[48,49]

The strongest Raman features detected in this region (at 2913 and 2977 cm^{-1}) were assigned by Mureinik and Scheuermann[42] to the symmetric and antisymmetric $\tilde{\nu}_{NH_3}$ modes, respectively. The same authors ascribed the doublet at 2807 and 2818 cm^{-1} to the $\tilde{\nu}_{CH_2}$ vibrations. However, further studies by McLachlan[44] and by Angeloni et al.[45] attributed the two higher-wavenumber bands (at 2913 and 2977 cm^{-1}) to $\tilde{\nu}_{CH_2}$, while the three $\tilde{\nu}_{NH_3}$ modes were assigned to the low-intensity features at 3025, 2998, and 2899 cm^{-1}. The present results show that N-deuteration, while hardly affecting the strong bands at 2913 and 2977 cm^{-1}, leads to the disappearance of the spectral features at 2818, ≈ 2899, and 3025 cm^{-1}. Moreover, a significant intensity decrease is observed at 2807 cm^{-1}, while several combination modes also disappear from this region.

Furthermore, the force field calculations predict all three $\tilde{\nu}_{NH_3}$ modes to be of lower wavenumber than the $\tilde{\nu}_{CH_2}$ ones. Given that all N–H groups are involved in NH⋅⋅⋅Cl close contacts, there is no reason for one of the $\tilde{\nu}_{NH_3}$ modes to present a much higher wavenumber (more than 200 cm^{-1}) than the other two. Consequently, the 2913 and 2977 cm^{-1} bands are assigned to $\tilde{\nu}_{CH_2}$ modes, while the three $\tilde{\nu}_{NH_3}$ oscillators are ascribed to the bands at 2807, 2818, and ≈ 2899 cm^{-1}. This is in accordance with the expected behavior of this kind of linear

amines upon N-deuteration—the $\tilde{\nu}_{CH_2}$ modes being insensitive while the $\tilde{\nu}_{NH_3}$ modes are significantly shifted downward (by more than 700 cm^{-1}, according to the theoretical results; Table 2).

The FTIR spectrum profile of the $1,2\,NH_3\cdot Cl$ and $1,2\,ND_3\cdot Cl$ systems in this high-wavenumber region is even more difficult to analyze, due to the very large number of combination modes and overtones detected with a relatively high intensity (Figure 5). The absorptions between 2000 and 2100 cm^{-1} in the $1,2\,NH_3\cdot Cl$ spectrum have been ascribed to combination modes that involve δ_{NH_3} fundamentals, recorded at around 1600 cm^{-1}, and torsion vibrations of the NH_3 group.[48,49] Moreover, similar bands with much lower intensity were observed and assigned to combination modes between $\tilde{\nu}_{NH_3}$ and τ_{NH} (Figure 4). These combinations are known to be particularly sensitive to the hydrogen-bond network involving the diamine NH_3^{2+} terminal groups.[49] Additional bands up to ≈ 2800 cm^{-1} have also been assigned to other combination modes of the δ_{NH_3} oscillators with different fundamental vibrations (e.g., δ_{CH_2}, ρ_{NH_3}, δ_{NCC}).[45]

On the other hand, the occurrence of strong features between 2800 and 3200 cm^{-1} is characteristic of the infrared spectrum of primary amine salts.[48] However, in spite of the five fundamentals expected to occur in this region, a huge number of bands with significant intensity is observed, thus rendering the assignment extremely difficult, given that several combination modes and overtones occur in this wavenumber range.

The strongest absorptions at 2799, 2874, and 2899 cm^{-1} are assigned to the expected $\tilde{\nu}_{NH_3}$ vibrations, as these three features disappear upon N-deuteration. The corresponding $\tilde{\nu}_{ND_3}$ modes give rise to spectral features between 1900 and 2200 cm^{-1}, where several combination modes are also detected. Assuming, once again, that the most intense absorptions correspond to fundamental vibrations, the features at 2123, 2164, and 2185 cm^{-1} would be ascribed to the three $\tilde{\nu}_{ND_3}$ modes, with a downward shift factor of 1.32.

Assignment of the CH_2 stretching modes is particularly difficult due to the very large number of overlapping combination modes occurring in the same spectral range. N-deuteration, in turn, does not simplify this region of the spectrum. Both $\tilde{\nu}_{CH_2}$ vibrations are expected to occur in the high-wavenumber wing of the broad and strong spectral feature. The band at 2972 cm^{-1} is tentatively assigned to one of the $\tilde{\nu}_{CH_2}$ modes, assuming that the other occurs at a lower wavenumber and is overpowered by the combination modes.

Regarding the relative ordering of the symmetric and antisymmetric CH_2 and NH_3 stretching modes, the calculations predict both $\tilde{\nu}_{sCH_2}$ and $\tilde{\nu}_{sNH_3}$ as presenting lower wavenumbers than their antisymmetric counterparts in both the Raman and FTIR spectra. Thus, the bands at 2807 and 2799 cm^{-1} are assigned to the Raman- and IR-active $\tilde{\nu}_{sNH_3}$ modes, respectively, while the antisymmetric NH_3 stretching vibrations are considered to give rise to the bands at 2818 and 2899 cm^{-1} (Raman), and 2874 and 2899 cm^{-1} (FTIR). In turn, the Raman-active $\tilde{\nu}_{sCH_2}$ vibration, which is theoretically predicted to occur at 2980 cm^{-1}, is ascribed to the band at 2913 cm^{-1}. The antisymmetric counterpart,

theoretically predicted to occur at 3026 cm^{-1}, gives rise to the band at 2977 cm^{-1}. In the FTIR spectrum, only one $\tilde{\nu}_{CH_2}$ mode appears, the other one being overpowered by the combination modes at lower wavenumbers, as previously referred to. Since the theoretical calculations predict a higher wavenumber for the antisymmetric mode than for the symmetric one, the band at 2972 cm^{-1} is tentatively assigned to the $\tilde{\nu}_{asCH_2}$ oscillator.

3. Conclusions

Herein, a structural and vibrational analysis was performed for 1,2-ethylenediamine dihydrochloride in the solid state by using both Raman and FTIR spectroscopy, coupled to ab initio calculations. Several theoretical molecular models were proposed to accurately represent this system and yield the best possible agreement with the experimental data (X-ray structures and vibrational frequencies) obtained for this linear diamine.

From the results obtained for the different molecular models proposed (*models 1 to 5*), it becomes evident that *models 1 to 4* are far from acceptable for an accurate description of this type of ionic nitrogen-containing systems. Actually, the extension of the theoretical representation up to *model 4*, although it leads to a clear improvement of several structural parameters, is also responsible for a significant overestimation of the NH$_{(2,3)}$···Cl close contacts. Furthermore, the huge increase in computational effort when going from *model 3* to *model 4* reinforces the conclusion that this latter approach becomes prohibitive for the study of similar larger diamines (e.g., [H$_3$N(CH$_2$)$_n$NH$_3$)]$^{2+}$·2Cl$^-$, $n=3$–10 and $n=12$).

Model 5 is undoubtedly the most suitable one, yielding a quite good compromise between accuracy and computational requirements. This molecular model, while being very simple, mimics the core structure of crystalline 1,2NH$_3$·Cl: it consists of one diamine cation surrounded by six chloride ions, each Cl$^-$ anion points to one N—H bond and establishes an intermolecular N—H···Cl close contact, as predicted by the reported X-ray results.[40,41]

On the whole, it was found that both the number and spatial orientation of the chloride counterions are essential for an accurate theoretical description of this kind of polycationic diamine systems in the solid state. The results indicate that both geometry and vibrational theoretical simulations based on *model 5* are quite accurate if the intrinsic limitations of the method (condensed phase vs. isolated molecule) are kept in mind. Also, it was found that the predicted $\Delta\tilde{\nu}$ values obtained upon N-deuteration are in good agreement with the experimentally observed ones. Moreover, the theoretical force field calculations were shown to be particularly useful for clarifying several reported controversies regarding the vibrational assignment of solid 1,2NH$_3$·Cl.

Experimental Section

Raman and FTIR spectroscopy: Room-temperature FT-Raman spectra were recorded on an RFS-100 Bruker FT-spectrometer, using an Nd:YAG laser with an excitation wavelength of 1064 nm. Each spectrum was the average of three repeated measurements of 150 scans at 2 cm^{-1} resolution. To observe the low-wavenumber vibrational modes (below 100 cm^{-1}), Raman data was also obtained on a Spex Ramalog 1403 double spectrometer (focal distance 0.85 m, aperture *f*/7.8) equipped with holographic gratings of 1800 grooves mm^{-1} and a detector assembly containing a thermoelectrically cooled Hamamatsu R928 photomultiplier tube, which operates with slits of 320 μm. The light source was a Coherent Innova 90 argon ion laser, whose output at 514.5 nm was adjusted to provide 90 mW at the sample position. The spectra were recorded with a wavenumber increment of 1 cm^{-1} and an integration time of 1 s (approximate scan speed 1 cm^{-1} s^{-1}), and corresponded to an average of two scans. In all experiments, the samples were sealed in Kimax glass tubes of 0.8 mm inner diameter.

Room-temperature FTIR spectra were recorded on an IFS 55 spectrometer, using a Golden Gate single-reflection diamond ATR system, which required no sample preparation. All spectra are the average of three counts, with 128 scans each, at 2 cm^{-1} resolution. The bands below 600 cm^{-1} were inaccessible due to apparatus limitations.

Ab initio MO calculations: The ab initio molecular orbital calculations were carried out using the GAUSSIAN 98 program.[50] All calculations were performed within the density functional theory (DFT) approach, using the B3LYP method,[51–56] which includes a mixture of Hartree–Fock (HF) and DFT exchange terms. The gradient-corrected correlation functional was used[57,58] (parameterized after Becke[59,60]), along with the double-zeta split valence basis set 6–31G*.[61] Molecular geometries were fully optimized by the Berny algorithm, using redundant internal coordinates.[62] Only the all-*trans* geometries (all skeletal dihedral angles equal to 180°) were considered, as the crystal packing of the diamine salts under study was not compatible with conformations displaying other configurations. The harmonic vibrational force fields were calculated for each optimized structure at the same theory level. The wavenumbers above 500 cm^{-1} were scaled by a factor of 0.9614, according to Scott and Radom.[63]

The vibrational assignments were based on the visualization of the atomic displacements, using the GaussView package,[64] and on the results from PED calculations, carried out with a modified version of the QCPE#576 program.[65] The force constants in Cartesian coordinates were transformed, via the FLINT program,[66] to independent internal coordinates defined according to the recommendations of Pulay et al.[67]

NBO analyses[68–70] were carried out for all optimized geometries to get a deeper insight into their electronic structures. Both the natural charges and the Wiberg bond indexes, based on the natural atomic order (NAO) basis set, were used to determine the nature of the hydrogen bond close contacts occurring within the systems studied.

As the main goal of the present work is to find an accurate molecular model for the representation of diamine salts in the solid state, five different models were considered. These are represented in Figure 1, along with the corresponding nomenclature used throughout the text: *model 1* (dicationic monomer); *model 2* (dicationic dichloride monomer); *model 3* (dicationic dichloride trimer); *model 4* (dicationic dichloride nonamer); *model 5* (central fragment of the 1,2NH$_3$·Cl reported crystal structure).[40,41]

Chemicals: 1,2-ethylenediamine dichloride was purchased from Sigma–Aldrich and used without further purification. The N-deuterated compound was obtained by mixing the dichloride salt with D$_2$O (ca. 10% excess), and distilling under vacuum, followed by purification through sublimation (this process was repeated at least three times).

[1] M. Auvinen, A. Passinen, L. C. Anderson, E. Holtta, *Nature* **1992**, *360*, 355.

[2] D. Guo, Z. Lu, *J. Gen. Physiol.* **2000**, *115*, 783.

[3] V. Vassileva, G. Ignatov, *Bulg. J. Plant Physiol.* **1999**, *25*, 49.

[4] S. Ramaswamy, M. R. N. Murthy, *J. Indian Inst. Sci.* **1994**, *74*, 591, and references therein.

[5] X. Xie, R. J. Gillies, E. W. Gerner, *J. Biol. Chem.* **1997**, *272*, 20 484.

[6] C. W. Tabor, H. Tabor, *Ann. Rev. Biochem.* **1984**, *53*, 749, and references therein.

[7] M. A. Medina, J. L. Urdiales, C. Rodriguez-Caso, F. J. Ramírez, F. Sánchez-Jiménez, *Crit. Rev. Biochem. Mol. Biol.* **2003**, *38*, 23.

[8] H. Deng, V. A. Bloomfield, J. M. Benevides, G. J. Thomas Jr., *Nucleic Acids Res.* **2000**, *28*, 3379.

[9] J. Ruiz-Chica, M. A. Medina, F. Sánchez-Jiménez, F. J. Ramírez, *Biophys. J.* **2001**, *80*, 443.

[10] J. Ruiz-Chica, M. A. Medina, F. Sánchez-Jiménez, F. J. Ramírez, *Biochem. Biophys. Res. Commun.* **2001**, *285*, 437.

[11] A. J. Ruiz-Chica, M. A. Medina, F. Sánchez-Jiménez, F. J. Ramírez, *J. Mol. Struct.* **2003**, *565/566*, 141.

[12] N. Korolev, A. P. Lynbartsev, A. Laaksonen, L. Nordenkiöld, *Biophys. J.* **2002**, *82*, 2860.

[13] M. Samiathan, T. Thomas, A. Shirahata, C. K. S. Pillai, T. J. Thomas, *Nucleic Acids Res.* **2002**, *30*, 3722.

[14] L. van Dam, N. Norolev, L. Nordenkiöld, *Nucleic Acids Res.* **2002**, *30*, 419.

[15] K. Nishioka, *Polyamines in Cancer: Basic Mechanisms and Clinical Approaches*, Springer-Verlag, Heidelberg, **1996**, and references therein.

[16] T. G. O'Brien, L. C. Megosh, G. Gilliard, A. P. Soler, *Cancer Res.* **1997**, *57*, 2630.

[17] G. G. Feuerstein, J. Szollsi, H. S. Basu, L. J. Marton, *Cancer Res.* **1992**, *52*, 6782.

[18] N. E. Davidson, H. A. Hahm, D. E. McCloskey, P. M. Woster, R. A. Casero Jr., *Endocr.-Relat. Cancer* **1999**, *6*, 69.

[19] H. Rauter, R. Di Domenico, E. Menta, A. Oliva, Y. Qu, N. Farrell, *Inorg. Chem.* **1997**, *36*, 3919, and references therein.

[20] M. P. M. Marques, T. Girão, M. C. Pedroso de Lima, A. Gameiro, E. Pereira, P. Garcia, *Biochim. Biophys. Acta, Mol. Cell Res.* **2002**, *1589*, 63.

[21] L. J. Teixeira, M. Seabra, E. Reis, M. T. Girão da Cruz, M. C. Pedroso de Lima, E. Pereira, M. A. Miranda, M. P. M. Marques, *J. Med. Chem.* **2004**, *47*, 2917.

[22] N. Farrell, Y. Qu, M. P. Hacker, *J. Med. Chem.* **1990**, *33*, 2179.

[23] P. Perego, L. Gatti, C. Caserini, R. Supino, D. Colangelo, R. Leone, S. Spinelli, N. Farrell, F. Zumino, *J. Inorg. Biochem.* **1999**, *77*, 59.

[24] C. Manzotti, G. Pratesi, E. Menta, R. di Domenico, E. Cavalleti, H. H. Fiebig, L. R. Kelland, N. Farrell, D. Polizzi, R. Suspiro, G. Pezzone, F. Zunino, *Clin. Cancer Res.* **2000**, *6*, 2626.

[25] C. Navarro-Ranninger, P. Amo-Oehoa, J. M. Pérez, V. M. González, J. R. Masagner, C. Alonso, *J. Inorg. Biochem.* **1994**, *53*, 177.

[26] P. Amo-Ochoa, V. M. González, J. M. Pérez, J. R. Masagner, C. Alonso, C. Navarro-Ranninger, *J. Inorg. Biochem.* **1996**, *64*, 287.

[27] T. Servidei, C. Ferlini, A. Riccardi, D. Meco, G. Scambia, G. Segni, C. Manzotti, P. Riccardi, *Eur. J. Cancer* **2001**, *37*, 930.

[28] J. M. Amatruda, D. H. Lockwood, *Biochim. Biophys. Acta* **1974**, *372*, 266.

[29] L. A. E. Batista de Carvalho, J. J. C. Teixeira-Dias, *J. Mol. Struct.* **1993**, *282*, 199.

[30] L. A. E. Batista de Carvalho, J. J. C. Teixeira-Dias, *J. Mol. Struct.* **1993**, *282*, 211.

[31] L. A. E. Batista de Carvalho, L. E. Lourenço, M. P. M. Marques, *J. Mol. Struct.* **1999**, *482/483*, 639.

[32] M. P. M. Marques, L. A. E. Batista de Carvalho, J. Tomkinson, *J. Phys. Chem.* **2002**, *A106*, 2473.

[33] Y.-L. Lam, H. H. Huang, *J. Mol. Struct.* **1997**, *412*, 141.

[34] B. Lakard, G. Herlem, B. Fahys, *J. Mol. Struct. (THEOCHEM)* **2002**, *584*, 15.

[35] S. J. Lee, B. J. Mhin, S. J. Cho, J. Y. Lee, K. S. Kim, *J. Phys. Chem.* **1994**, *98*, 1129.

[36] P. Bultinck, A. Goeminne, D. V. de Vondel, *J. Mol. Struct. (THEOCHEM)* **1995**, *339*, 1.

[37] S. Bondon, G. Wipff, *J. Mol. Struct. (THEOCHEM)* **1991**, *228*, 61.

[38] A. M. Amorim da Costa, M. P. M. Marques, L. A. E. Batista de Carvalho, *Vib. Spectrosc.* **2002**, *29*, 61.

[39] A. M. Amorim da Costa, M. P. M. Marques, L. A. E. Batista de Carvalho, *J. Raman Spectrosc.* **2003**, *34*, 357.

[40] T. Ashida, S. Hirokawa, *Bull. Chem. Soc. Jpn.* **1963**, *36*, 704.

[41] M. Bujak, L. Sikorska, J. Zalesli, *Z. Anorg. Allg. Chem.* **2000**, *626*, 2535.

[42] R. J. Mureinik, W. Scheuermann, *Spectrosc. Lett.* **1970**, *3*, 281.

[43] R. W. Berg, K. Rasmussen, *Spectrosc. Lett.* **1971**, *4*, 285.

[44] R. D. McLachlan, *Spectrochim. Acta* **1974**, *A30*, 985.

[45] L. Angeloni, E. Castellucci, M. P. Marzocchi, *Chem. Phys.* **1977**, *26*, 257.

[46] I. A. Oxton, O. Knop, *J. Mol. Struct.* **1978**, *43*, 17.

[47] L. A. E. Batista de Carvalho, A. M. Amorim da Costa, J. J. C. Teixeira-Dias, *J. Mol. Struct.* **1990**, *218*, 105.

[48] N. B. Colthup, L. H. Daly, S. E. Wiberley in *Introduction to Infrared and Raman Spectroscopy, 3rd Edition,* Academic Press Inc., San Diego, **1990**, p. 343.

[49] N. P. G. Roeges in *A Guide to the Complete Interpretation of Infrared Spectra of Organic Structures*, John Wiley & Sons, West Sussex, **1994**, pp. 83–87.

[50] *Gaussian 98*, Revision A.9, M. J. Frisch, G. W. Trucks, H. B. Schlegel, G. E. Scuseria, M. A. Robb, J. R. Cheeseman, V. G. Zakrzewski, J. A. Montgomery, Jr., R. E. Stratmann, J. C. Burant, S. Dapprich, J. M. Millam, A. D. Daniels, K. N. Kudin, M. C. Strain, O. Farkas, J. Tomasi, V. Barone, M. Cossi, R. Cammi, B. Mennucci, C. Pomelli, C. Adamo, S. Clifford, J. Ochterski, G. A. Petersson, P. Y. Ayala, Q. Cui, K. Morokuma, D. K. Malick, A. D. Rabuck, K. Raghavachari, J. B. Foresman, J. Cioslowski, J.V. Ortiz, A. G. Baboul, B. B. Stefanov, G. Liu, A. Liashenko, P. Piskorz, I. Komaromi, R. Gomperts, R. L. Martin, D. J. Fox, T. Keith, M. A. Al-Laham, C. Y. Peng, A. Nanayakkara, M. Challacombe, P. M. W. Gill, B. Johnson, W. Chen, M. W. Wong, J. L. Andres, C. Gonzalez, M. Head-Gordon, E. S. Replogle, J. A. Pople, Gaussian Inc., Pittsburgh PA, **1998**.

[51] T. V. Russo, R. L. Martin, P. J. Hay, *J. Phys. Chem.* **1995**, *99*, 17 085.

[52] A. Ignaczak, J. A. N. F. Gomes, *Chem. Phys. Lett.* **1996**, *257*, 609.

[53] F. A. Cotton, X. Feng, *J. Am. Chem. Soc.* **1997**, *119*, 7514.

[54] T. Wagener, G. Frenking, *Inorg. Chem.* **1998**, *37*, 1805.

[55] A. Ignaczak, J. A. N. F. Gomes, *J. Electroanal. Chem.* **1997**, *420*, 209.

[56] F. A. Cotton, X. Feng, *J. Am. Chem. Soc.* **1998**, *120*, 3387.

[57] C. Lee, W. Yang, R. G. Parr, *Phys. Rev.* **1988**, *B37*, 785.

[58] B. Miehlich, A. Savin, H. Stoll, H. Preuss, *Chem. Phys. Lett.* **1989**, *157*, 200.

[59] A. Becke, *Phys. Rev.* **1988**, *A38*, 3098.

[60] A. Becke, *J. Chem. Phys.* **1993**, *98*, 5648.

[61] P. C. Hariharan, J. A. Pople, *Theor. Chim. Acta* **1973**, *28*, 213.

[62] C. Peng, P. Y. Ayala, H. B. Schlegel, M. J. Frisch, *J. Comp. Chem.* **1996**, *17*, 49.

[63] A. P. Scott, L. Radom, *J. Phys. Chem.* **1996**, *100*, 16 502.

[64] Æ. Frisch, A. B. Nielsen, A. J. Holder, *GaussViewW* (version 2), Gaussian Inc., Pittsburgh, USA, **2000**.

[65] D. F. McIntosh, M. R. Peterson, *General Vibrational Analysis System*, **QCPE#576**, Toronto, **1989**.

[66] J. F. Arenas, J. T. López-Navarrete, J. I. Marcos, J. C. Otero, *Spectrochim. Acta* **1986**, *42A*, 1343.

[67] P. Pulay, G. Fogarasi, F. Pang, J. E. Boggs, *J. Am. Chem. Soc.* **1979**, *101*, 2550.

[68] E. D. Glendening, A. E. Reed, J. E. Carpenter, F. Weinhold, *NBO 3.0 Program Manual*, Gaussian Inc., Pittsburgh, PA, **1996**.

[69] A. E. Reed, R. B. Weinstock, F. Weinhold, *J. Chem. Phys.* **1985**, *83*, 735.

[70] A. E. Reed, L. A. Curtis, F. A. Weinhold, *Chem. Rev.* **1988**, *88*, 899.